Supporting Information

Shi and Ruvkun 10.1073/pnas.1202421109

SI Materials and Methods

***Caenorhabditis elegans* Strains.** The following strains were used in this study:

N2: wild type
VT460: *lin-4(e912)/mnC1 dpy-10(e128) unc-52(e444) II*
GR1575: *lin-14(n355n679) X*
RG365: *him-1(e879) I; veIs13[col-19::gfp; rol-6(su1006)] V*
GR1445: *veIs13 V; let-7(mg279) X*
RB574: *alg-2(ok304) II*
VC446: *alg-1(gk214) X*
MH2385: *ain-1(ku322) X*
GR1332: *let-7(mg279) X*
GR1694: *hmgr-1(tm4368) III; veIs13 V; let-7(mg279) X*
GR1696: *hmgr-1(tm4368) III*
GR1716: *xbp-1(zc12) III; veIs13 V; let-7(mg279) X*
BW1932: *ctIs39[hbl-1::gfp, pRF4(rol-6(su1006))]*
GR1737: *hmgr-1(tm4368) III; ctIs39*
GR1738: *lin-41(ma104) I; veIs13 V*
GR1739: *lin-42(n1089) II; veIs13 V*
GR1740: *lin-28(n719) I; veIs13 V*
Is[alg-1p::gfp::alg-1] (from the Slack laboratory, Yale University, New Haven, CT)
Is[ain-1::gfp, dsred2::alg-1] (from the Han laboratory, University of Colorado, Boulder, CO)
GR1709: *otIs114[lim-6p::gfp + rol-6(su1006)] I; lsy-6(ot150) V; nre-1(hd20) lin-15b(hd126) X*
GR1710: *otIs114[lim-6p::gfp + rol-6(su1006)] I; nre-1(hd20) lin-15b(hd126) X*
GR1832: *mgSi21[alg-1p::HA::alg-1::alg-1-3′ UTR] IV; alg-1(gk214) X*

Feeding RNAi. In addition to the RNAi clones used in Table S3, the following gene was knocked down by feeding RNAi using the Ahringer RNAi library (1): *F48F7.1* (*alg-1*/Argonaute), which probably also targets *alg-2* due to the high sequence similarity, and therefore is referred to as *alg-1/2* RNAi. HT115 bacteria carrying the empty vector L4440, which expresses dsRNA homologous to no worm gene, were used as a control. Bacterial clones were cultured at 37 °C for 15 h before seeding the RNAi plates. After induction of dsRNA for 24 h at room temperature, worms were placed on RNAi plates.

LIN-14 Western Blots. Because *hmgs-1* is an essential gene for fertility, we applied a mild gene knockdown by feeding the parental (P_0) animals with *Escherichia coli* expressing *hmgs-1* dsRNA diluted with control *E. coli* expressing dsRNA homologous to no worm gene, starting at the fourth (L4) larval stage. Embryos were isolated from the P_0 animals to synchronize their progeny by hatching in the absence of food. A fraction of synchronized L1s were flash-frozen in liquid nitrogen and others were fed on plates seeded with undiluted RNAi bacteria at 20 °C and collected after 20 and 23 h. At 24 h, worms were visually inspected to ensure they were all at the early L2 stage by counting the number of germ cells, the divided intestinal nuclei, and disappearance of L1 alae. Worm lysate preparation and LIN-14 Western blotting were performed as previously described (2). Blots were reprobed with actin antibody (Abcam; ab3280) as loading control.

Quantification of MicroRNA by Real-Time PCR. The following procedure was adapted from ref. 3. RNA was isolated, DNase-treated, and polyadenylated by poly(A) polymerase. An adapter primer containing a unique 5′ sequence and 12 Ts and ending in VN-3′ was used to make cDNA. This anchors the adapter to the beginning of the poly(A) tail by virtue of the VN-3′ nucleotides (V = A, C, or G; *n* = A, T, C, or G). The cDNA is then amplified with a forward primer based on the entire tested microRNA (miRNA) sequence and a reverse primer complementary to the adapter. The PCR amplification was monitored by SYBR Green incorporation, and a corresponding threshold cycle (C_T) was obtained. The quantity of miRNA, relative to two internal reference genes, U6 and 18s rRNA, was calculated using the formula $2^{-\Delta CT}$, where $\Delta C_T = (C_{T\ \mathrm{miRNA}} - C_{T\ \mathrm{reference}})$. For each miRNA, the result was shown relative to its level in wild-type animals treated with control RNAi. The mean and SD were calculated from three biological replicates.

ALG-1 Immunoprecipitation. ALG-1 was purified from synchronized L4-stage *alg-1(gk214)* mutants rescued with an HA-ALG-1 single-copy construct. About 0.5 mL of worms was flash-frozen in liquid nitrogen, followed by grinding with a mortar and pestle. An equal volume of cell lysis buffer [50 mM Tris·HCl (pH 7.4), 100 mM KCl, 2.5 mM $MgCl_2$, 0.1% Nonidet P-40, 0.5 mM PMSF, 1 Complete proteinase inhibitor tablet (Roche)/15 mL, 40 U/mL RNaseOUT (Invitrogen)] was added, and the lysate was homogenized on a head-to-tail rotor for 15 min. Debris was spun down in a tabletop centrifuge at 12,000 × g for 5 min at 4 °C. The cell lysate was precleared by adding 20 μL protein A agarose bead slurry (Roche) and rotating for 10 min. The cleared lysate was incubated with 3 μL HA antibody (clone 12CA5; Roche) for 20 min and then 100 μL protein A agarose bead slurry for 20 min at 4 °C. The beads were then washed eight times for 40 min in total. Ten percent of the immunoprecipitation (IP) sample was used for Western blot analysis. Ninety percent of the IP sample was treated with proteinase K (1.0 μg/μL; Ambion) at 65 °C for 15 min. RNA was extracted with phenol-chloroform and subjected to miRNA real-time PCR analysis.

1. Kamath RS, et al. (2003) Systematic functional analysis of the *Caenorhabditis elegans* genome using RNAi. *Nature* 421:231–237.
2. Reinhart BJ, Ruvkun G (2001) Isoform-specific mutations in the *Caenorhabditis elegans* heterochronic gene lin-14 affect stage-specific patterning. *Genetics* 157(1):199–209.
3. Shi R, Chiang VL (2005) Facile means for quantifying microRNA expression by real-time PCR. *Biotechniques* 39:519–525.

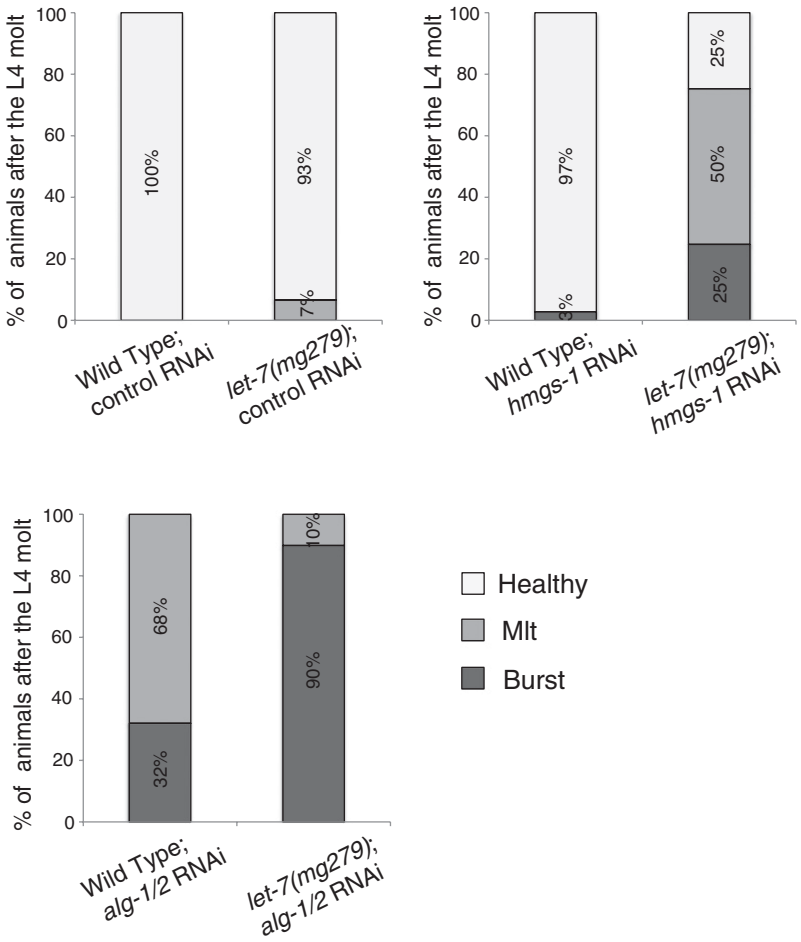

Fig. S1. The percentage of molting-defective (Mlt) and burst animals upon a mild knockdown of *hmgs-1* or *alg-1/2* by diluted RNAi is enhanced by the *let-7 (mg279)* mutation. Shown are the percentage of healthy, Mlt, and burst animals after the L4-to-adult molt in wild type and *let-7(mg279)* mutants. Mlt animals retain eggs following a defective molt and are eventually consumed by their progeny. Animals were fed starting at L1 with *E. coli* expressing *hmgs-1* or *alg-1/2* dsRNA diluted with control *E. coli* expressing a benign dsRNA and scored after the L4-to-adult molt. The percentage of burst and Mlt animals is enhanced in the *let-7(mg279)* mutant compared with wild type when fed with diluted *hmgs-1* or *alg-1/2* RNAi.

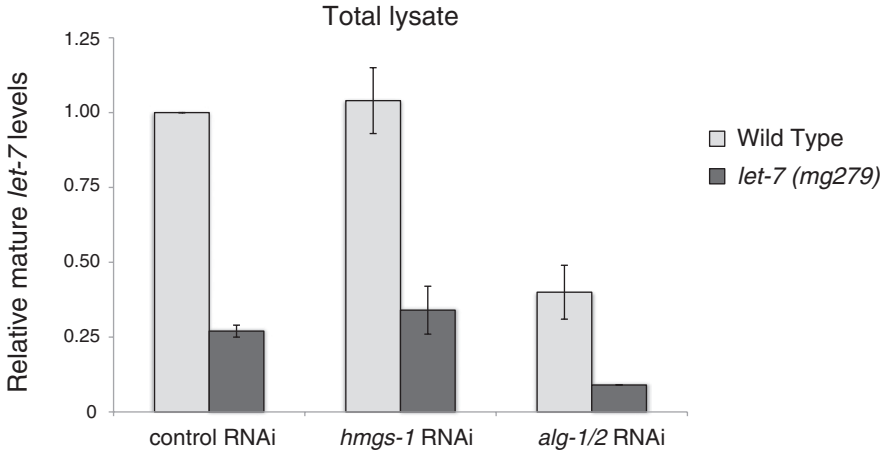

Fig. S2. Inactivation of *hmgs-1* does not reduce *let-7* miRNA levels in the sensitized *let-7(mg279)* mutant background. The mature *let-7* level was measured by real-time PCR and is shown relative to its level in wild-type animals treated with control RNAi. Compared with stage-matched wild-type animals, the *let-7 (mg279)* mutant has a reduced level of mature *let-7* miRNA. Inactivation of *alg-1/2* further reduces the *let-7* miRNA level; however, inactivation of *hmgs-1* does not reduce the *let-7* miRNA level even in the sensitized *let-7(mg279)* mutant. The mean and SD were calculated from three biological replicates. Error bars represent SEM.

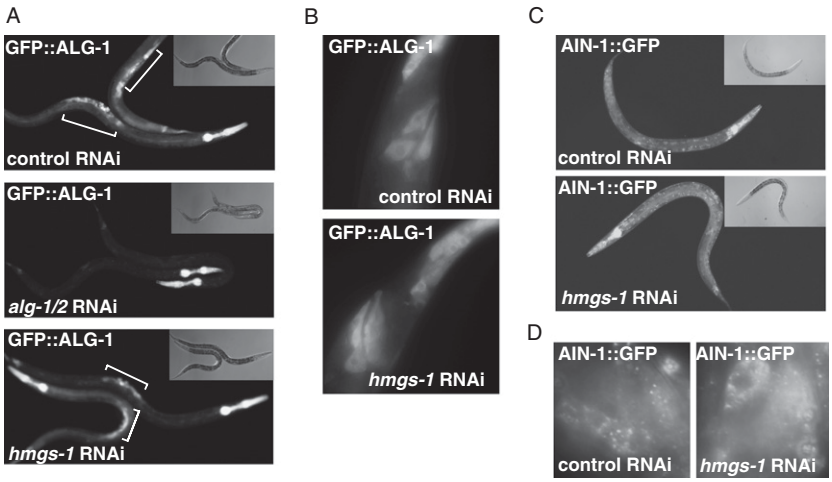

Fig. S3. *hmgs-1* does not regulate the overall expression pattern or subcellular localization of ALG-1/Argonaute and AIN-1/ALG-1 interacting proteins. (*A*) Global GFP::ALG-1 expression in control, *alg-1/2*, or *hmgs-1* RNAi-treated L4 animals. Brackets indicate the vulval and somatic gonadal expression of GFP::ALG-1 in control and *hmgs-1* but not *alg-1/2* RNAi-treated animals. (*Insets*) Nomarski images. (*B*) Shown are several cells in the tail region. GFP::ALG-1 is largely diffuse in the cytoplasm. This pattern is not affected upon RNAi depletion of *hmgs-1*. (*C*) AIN-1::GFP is ubiquitously expressed in L4 animals, with the highest expression in the head neurons. This pattern is not affected upon RNAi depletion of *hmgs-1*. (*Insets*) Nomarski images. (*D*) Shown are several cells in the tail region. AIN-1::GFP exhibits punctate cellular localization, and this pattern is not affected upon RNAi depletion of *hmgs-1*.

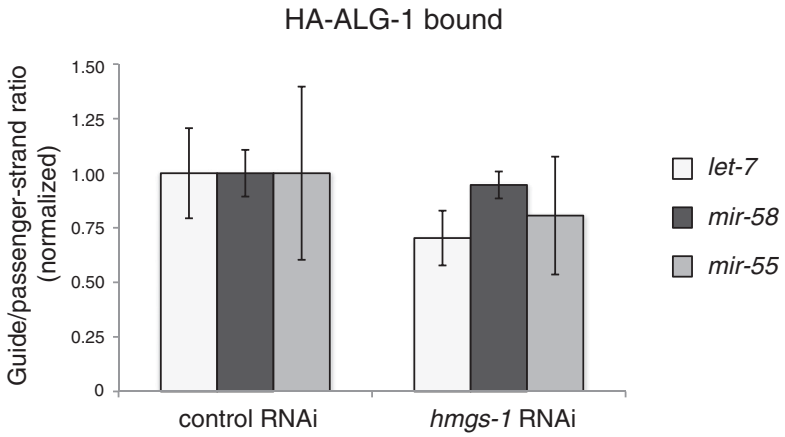

Fig. S4. The unwinding of the miRNA duplex is not affected by inactivation of *hmgs-1*. The guide:passenger strand ratio of *let-7*, *mir-58*, and *mir-55* was unaltered after inactivation of *hmgs-1*. HA-ALG-1 was immunoprecipitated, and then the levels of associated guide and passenger strand of *let-7*, *mir-58*, and *mir-55* were measured by real-time PCR. The results were normalized to the mean guide:passenger strand ratio in control RNAi-treated animals. The mean and SD were calculated from three biological replicates. Error bars represent SEM.

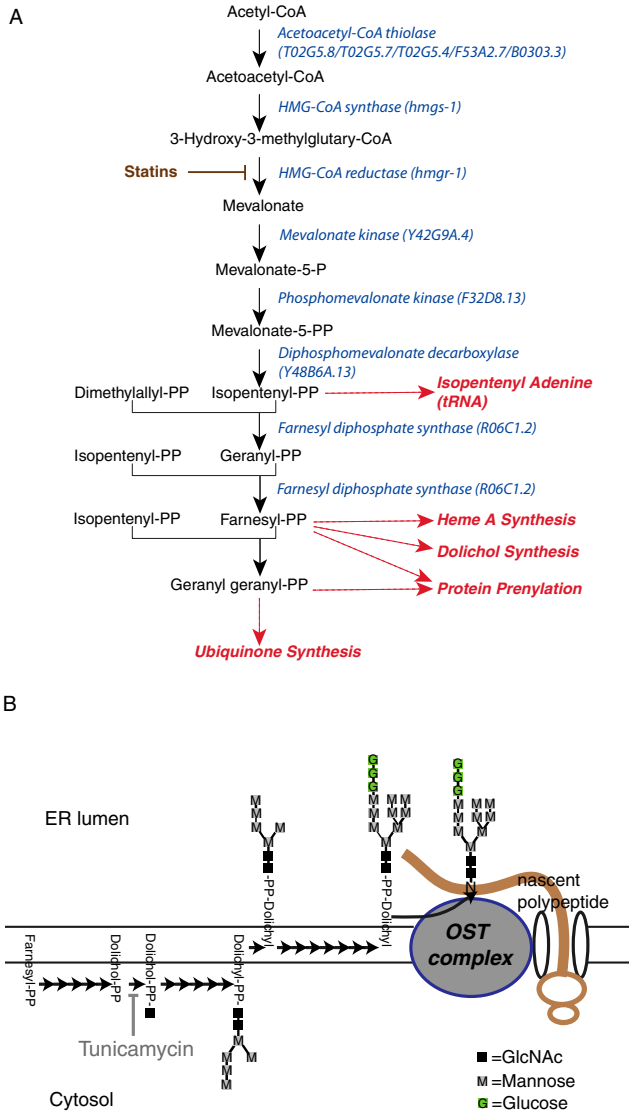

Fig. S5. Dolichol phosphate is synthesized from the mevalonate pathway and has a role in protein *N*-linked glycosylation. (*A*) Diagram of the *C. elegans* mevalonate pathway. (*B*) Dolichol phosphate synthesized from the mevalonate pathway serves as the lipid carrier of the oligosaccharide moiety destined for protein *N*-linked glycosylation. The transfer of oligosaccharide to an asparagine residue on a nascent polypeptide is catalyzed by the oligosaccharyltransferase (OST) complex on the endoplasmic reticulum (ER) membrane. Tunicamycin blocks the reaction of UDP-GlcNAc and dolichol phosphate in the first step of the dolichol pathway.

A

Gene Inactivation	Description	*hsp-4::gfp* expression	Defect in down-regulation of *hbl-1::gfp* [% (n)][a]	Defect in *col-19::gfp* expression [% (n)][b]	
				let-7(mg279)	*xbp-1(zc12); let-7(mg279)*
control		very low	0% (12)	13% (195)	0% (110)
Y54E10BR.5	signal peptidase	high	0% (12)	83% (86)	0% (88)
arf-3	ADP-ribosylation factor related protein	high	0% (12)	80% (85)	72% (100)
fat-6	delta-9 fatty acid desaturase	high	0% (8)	10% (80)	65% (82)
fah-1	putative fumarylacetoacetate hydrolase	medium	0% (10)	38% (77)	0% (87)
pdi-3	disulfide isomerase	medium	0% (12)	87% (83)	0% (90)
sams-1	S-adenosylmethionine synthetase	high	nd	6% (73)	0% (82)
tkt-1	Transketolase	high	nd	1% (100)	0% (87)
ero-1	ER-associated oxidoreductin	high	nd	10% (90)	0% (83)

B

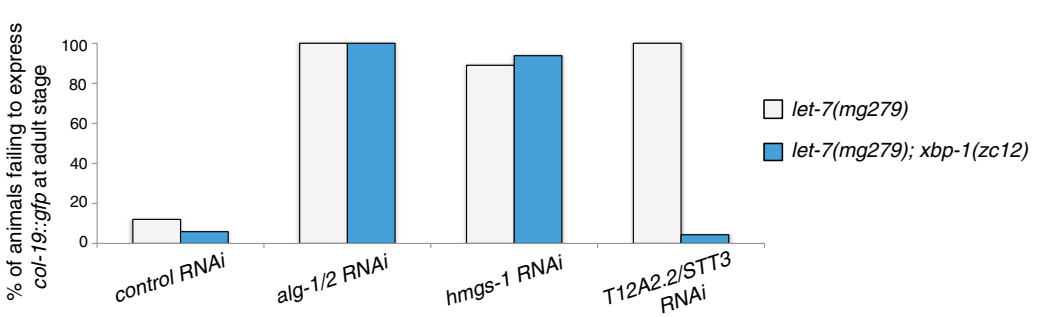

C

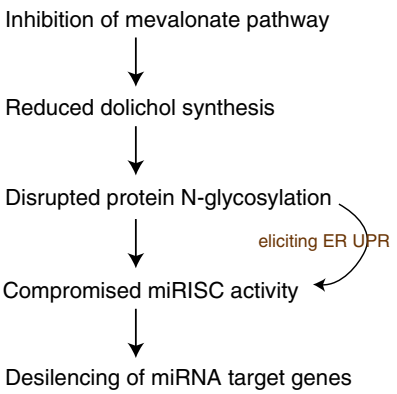

Fig. S6. Induction of ER stress mildly compromises *let-7* activity. (*A*) Inactivation of genes required for ER homeostasis causes up-regulation of *hsp-4/BiP::gfp*, the hallmark of ER stress. These gene inactivations do not cause a defect in the down-regulation of *hbl-1::gfp* at the L3 stage. However, a subset of gene inactivations causes *let-7(mg279)* mutant animals to fail to express *col-19::gfp* in hyp7 cells at the adult stage. In some but not all cases, this defect of *col-19::gfp* expression can be suppressed by the *xbp-1(zc12)* mutation. nd, not determined. [a]The expression of *hbl-1::gfp* in hyp7 cells was scored at the late L3 stage, and the percentage of animals having derepressed *hbl-1::gfp* is indicated. [b]The expression of *col-19::gfp* was scored at the adult stage, and the percentage of animals failing to express *col-19::gfp* in hyp7 cells is indicated. (*B*) Shown is the percentage of animals failing to express *col-19::gfp* in hyp7 cells at the adult stage. The *xbp-1(zc12)* mutation suppresses the failure of *col-19::gfp* expression in *T12A2.2/STT3* RNAi-treated *let-7(mg279)* mutants. However, *xbp-1(zc12)* does not suppress the failure of *col-19::gfp* expression caused by the inactivation of *alg-1/2* or *hmgs-1*. (*C*) The dolichol phosphate/protein *N*-glycosylation output of the mevalonate pathway is required in the miRNA repression of target mRNAs in *C. elegans*. miRISC, miRNA-induced silencing complex.

Table S1. Effect of *hmgs-1* inactivation on hypodermal cell fate speciation

		% of animals having adult alae*			
Strain	RNAi	No alae	Gapped	Complete	*n*
Wild type	Control	0	0	100	30
Wild type	*hmgs-1*	9	3	88	32
alg-1(gk214)	Control	45	55	0	20
alg-1(gk214)	*hmgs-1*	100	0	0	20
alg-2(ok304)	Control	0	0	100	15
alg-2(ok304)	*hmgs-1*	21	29	50	24
ain-1(ku322)	Control	10	38	52	21
ain-1(ku322)	*hmgs-1*	67	28	5	21

*The percentages of animals having no/gapped/complete alae structures were assessed after the L4-to-adult molt; only one side of each animal was assayed.

Table S2. Mevalonate supplementation rescues gene inactivation of *hmgs-1*

RNAi	No supplementation	55 μg/mL cholesterol	2 mM mevalonate
Control RNAi	Healthy gravid adult	Healthy gravid adult	Healthy gravid adult
alg-1/2 RNAi	Burst	Burst	Burst
hmgs-1 RNAi	Burst	Burst	Healthy gravid adult (complete rescue)

Table S3. Phenotypes of gene inactivations in the *let-7(mg279); [col-19::gfp]* background

Gene targeted*	Locus	Description	Phenotypes in P_0 animals†	Phenotypes in F_1 animals‡
Mevalonate pathway				
T02G5.8	*kat-1*	Acetyl-CoA acetyltransferase		
T02G5.7		Acetyl-CoA acetyltransferase		
T02G5.4		Acetyl-CoA acetyltransferase		
F53A2.7		Acetyl-CoA acetyltransferase		
B0303.3		Acetyl-CoA acetyltransferase		
F25B4.6	*hmgs-1*	HMG-CoA synthase	Burst and sterile; fail to express *col-19::gfp*	nd
F08F8.2	*hmgr-1*	HMG-CoA reductase		Weak *col-19::gfp*
Y42G9A.4	*mvk-1*	Mevalonate kinase		
Y48B6A.13		Mevalonate pyrophosphate decarboxylase		
R06C1.2	*fdps-1*	Polyprenyl synthetase		Weak *col-19::gfp*
Protein prenylation				
R02D3.5	*fnta-1*	Farnesyltransferase, α subunit		Burst
F23B12.6	*fntb-1*	β subunit of farnesyltransferase		
Y48E1B.3		Geranylgeranyltransferase type I, β subunit		
M57.2		Geranylgeranyltransferase type II, α subunit		Arrested at L3
B0280.1	*ggtb-1*	Geranylgeranyltransferase type II, β subunit		
Coenzyme Q biosynthesis				
C24A11.9	*coq-1*	*Trans*-prenyltransferases		Arrested at L2
F57B9.4	*coq-2*			
Y57G11C.11	*coq-3*			
K07B1.2	*coq-6*			
ZC395.2	*clk-1*			
Dolichol synthesis and *N*-glycosylation				
Y60A3A.14		ALG7 homolog		Pale-looking, weak *col-19::gfp*
R10D12.12		UDP-*N*-acetylglucosamine transferase subunit ALG13 homolog		
M02B7.4		UDP-*N*-acetylglucosamine transferase subunit ALG14 homolog		
T26A5.4		ALG1 homolog		
F09E5.2		ALG2 homolog		
B0361.8		ALG11 homolog		
K09E4.2		Dolichyl-P-Man:Man(5)GlcNAc(2)-PP-dolichyl mannosyltransferase		
C14A4.3		Mannosyltransferase ALG9 homolog		
ZC513.5		Mannosyltransferase ALG12 homolog		
C08B11.8		Glucosyltransferase ALG6 homolog		
C08H9.3		Glucosyltransferase ALG8 homoolog		
T24D1.4	*tag-179*	α-1,2 glucosyltransferase ALG10 homolog		
T22D1.4		Oligosaccharyltransferase, α subunit (ribophorin I)	Fail to express *col-19::gfp*	nd
M01A10.3	*ostd-1*	Oligosaccharyltransferase subunit; ortholog of yeast SWP1, human ribophorin II	Fail to express *col-19::gfp*	nd
T09A5.11	*ostb-1*	Oligosaccharyltransferase subunit; ortholog of yeast WBP1, human OST48	Fail to express *col-19::gfp*	nd

Table S3. Cont.

Gene targeted*	Locus	Description	Phenotypes in P_0 animals†	Phenotypes in F_1 animals‡
F57B10.10	*dad-1*	Oligosaccharyltransferase subunit; ortholog of yeast OST2, human DAD-1	Fail to express *col-19::gfp*	nd
T12A2.2		Oligosaccharyltransferase, STT3 subunit	Fail to express *col-19::gfp*	nd
Heme A and heme O biosynthesis				
Y46G5A.2		Protoheme IX farnesyltransferase		
T06D8.5		Cytochrome oxidase assembly factor COX15		
tRNA isopentenylation				
ZC395.6	*gro-1*	tRNA isopentenylpyrophosphate transferase		

If animals appeared WT after RNAi, cell is left empty. nd, not determined.
*The gene targeted by the RNAi clone was confirmed by sequencing.
†RNAi was initiated starting at the L1 stage, and the phenotypes were scored after the L4-to-adult molt.
‡RNAi was initiated starting at the L1 stage of P_0 animals, and the phenotypes were scored in progeny. However, the phenotypes were not determined if the RNAi caused lethality/sterility in P_0 animals.